One-phonon-assisted electron Raman scattering in quantum well wires and free-standing wires

2000 J. Phys.: Condens. Matter 12 7983

(http://iopscience.iop.org/0953-8984/12/36/312)

J. Phys.: Condens. Matter **12** (2000) 7983–7998. Printed in the UK PII: S0953-8984(00)12192-7

One-phonon-assisted electron Raman scattering in quantum well wires and free-standing wires

J M Bergues†‖, R Betancourt-Riera‡, R Riera§ and J L Marín§

† Departamento de Física de la Universidad de Sonora, Apartado Postal 1626, 83000 Hermosillo, Sonora, Mexico

‡ Departamento de Física de la Universidad de Oriente, Apartado 90500, Santiago de Cuba, Cuba

§ Centro de Investigación en Física, Universidad de Sonora, Apartado Postal 5-088, 83190 Hermosillo, Sonora, Mexico

Received 1 March 2000, in final form 14 July 2000

Abstract. The differential cross section for an electron Raman scattering process in a semiconductor quantum well wire (QWW) and in a free-standing wire of cylindrical geometry involving phonon-assisted transitions is calculated for $T = 0$ K. A complete description of the phonon modes of cylindrical structures embedded in another material, including a correct treatment of the mechanical and electrostatic matching conditions at the surface, is presented. We consider the Fröhlich interaction to illustrate the theory for a GaAs/AlAs system. Electron states are considered to be confined within a QWW with finite and infinite potential barriers. We also assume single parabolic conduction and valence bands. The emission spectra are discussed for different scattering configurations and the selection rules for the processes are also studied. Singularities in the spectra are found and interpreted.

1. Introduction

The advances in fabrication of new electro-optical devices based on low-dimensional systems have reinforced the great interest in the investigation of semiconductor nanostructures such as quantum wells, quantum dots, superlattices and quantum well wires, which are usually made from weakly ionic materials (like GaAs/AlAs). Such nanostructures might constitute the basis for an alternative class of solid-state lasers and transport and optoelectronic devices.

Polar optical oscillations in such systems play an important role in many physical processes, especially in the long-wavelength limit. One of the most important mechanisms of electron, hole and exciton scattering in these structures is through optical phonon emission and absorption, which has led to many studies being made of the effects of the reduced dimensionality on the phonon modes. A continuum theory of optical phonons in quantum well wires (QWW) and free-standing wires (FSW) was developed in [1–4]. The general principles and the underlying formalism have been applied [1] to determine the optical modes, as well as the dispersion relation curves and the electron–phonon interaction Hamiltonian. In reference [1] the dispersion was illustrated for phonon modes with $n = 0$, 1 and 2.

Raman scattering experiments are well known to provide a powerful tool for the investigation of different physical properties of semiconductor nanostructures [5–7]. In particular, the electronic structure of semiconductor materials and nanostructures can be thoroughly investigated by considering different polarizations for the incident and emitted

‖ On leave from: Departamento de Física de la Universidad de Oriente, Apartado 90500, Santiago de Cuba, Cuba.

0953-8984/00/367983+16$30.00

radiation [5, 8]. In connection with this kind of experiment, the calculation of the differential cross section (DCS) for electron Raman scattering (ERS) remains a rather interesting and fundamental issue as regards achieving a better understanding of the synthetic semiconductor nanostructures characterized by their mesoscopic dimensions [9–14].

Among the various Raman scattering processes involved in this kind of research, the ERS seems to be a particularly useful technique which provides direct information about the energy band structure and the optical properties of the systems investigated. ERS is qualitatively explained as a three-step process. In the first step, the system absorbs a photon from the incident radiation and an electron–hole pair (EHP) is created in a virtual state (after an interband electron transition); in the second step, the electron and the hole move independently of each other, emitting an optical phonon and performing intraband transitions. In the last step, the electron and the hole move independently of each other emitting secondary-radiation photons and performing an interband transition [14]. In the final state an EHP, a phonon of frequency ω_{nm} and a photon of frequency ω_s appear in a real state of system, which is thus left in an excited state.

Singularities are usually found in the DCS for ERS and they are related to interband and intraband transitions. The latter result strongly depends on the scattering configurations, i.e., the structure of the singularities changes when the photon polarization is modified [15]. This peculiar feature of ERS allows us to determine the subband structure of the system by direct inspection of the positions of the singularities in the spectra.

For bulk semiconductors, ERS has been studied in the presence of external magnetic and electric fields [16–19]. For the case of the quantum well, preliminary results were reported in [20]. The aim of this article is to study ERS in cylindrical QWW and FSW, considering transitions assisted by photons and phonons. We assume that the electron is partially or totally confined within the system. We consider parabolic bands and $T = 0$ K.

Cylindrical symmetry was chosen because it can be synthesized by several methods, namely, using porous silicon, zeolite cavities, molecular beam epitaxy with ionic attack and holographic nanolithography. The assumption that $T = 0$ K eliminates the phonon absorption term in the electron–phonon interaction Hamiltonian, but does not change the optical properties. The parabolic band approximation is commonly used for II–VI and III–V semiconductors when the description is near to the centre of the Brillouin zone in the reduced-zone scheme. Under these dynamical conditions and since the potential barriers do not imply interband transitions, the nanostructures can be treated within the envelope function and effective-mass approximations.

As regards the complexity of the valence band in III–V and II–VI semiconductor compounds, the contribution of band mixing is small in the confinement regime assumed in this work and this is consistent with previous treatments [21, 22]. When the excitation energy is close to the band-gap energy, the valence band structure is very important in the strong-confinement regime and just one conduction band can be assumed since the electronic contribution to the process is negligible, as has been pointed out recently by Fomin *et al* [23, 24]. However, this is not the case for the present work, because the excitation energy considered herein is much higher than the band-gap energy.

2. Model and applied theory

Let us briefly describe the model and the fundamental theory applied in our calculations. The QWW geometry is cylindrical with circular cross section of radius r_0 and length L. As was explained before, we consider a single conduction (valence) band split into a subband system due to electron confinement within the structure. The solution of the Schrödinger equation, in

the envelope function approximation, leads to

$$\Psi_{n_j m_j} = (2\pi L)^{-1/2} \exp(-\mathrm{i}(n_j\phi + k_{zj}z))u_j \begin{cases} A J_{n_j}\left(k_{xj}\dfrac{r}{r_0}\right) & r < r_0 \\ B K_{n_j}\left(k_{yj}\dfrac{r}{r_0}\right) & r > r_0 \end{cases} \tag{1}$$

with

$$B = \frac{J_{n_j}(k_{xj})}{K_{n_j}(k_{yj})}A \qquad \text{and} \qquad A = \left\{ \left|\left|J_{n_j}(k_{xj})\right|\right|^2 + \left[\frac{\mu_2 k_{xj} J'_{n_j}(k_{xj})}{\mu_1 k_{yj} K'_{n_j}(k_{yj})}\right]^2 \left|\left|K_{n_j}(y)\right|\right|^2 \right\}^{-1/2} \tag{2}$$

where

$$k_{xj} = \sqrt{\frac{2\mu_1 E_{n_j m_j}}{\hbar^2}}r_0 \qquad k_{yj} = \sqrt{\frac{2\mu_2 (V_0 - E_{n_j m_j})}{\hbar^2}}r_0$$

and $j = 1$ (2) is used to denote the electron (hole). J_{n_j} and K_{n_j} are the Bessel and modified Bessel functions, μ_1 (μ_2) are the effective masses in the wire (surrounding medium) and V_0 represents the band offset. The states are described by the quantum numbers: $n_j = 0, 1, \ldots$; $m_j = 1, 2, \ldots$; and k_{zj}. The matching conditions require the continuity of the function Ψ and the current $(1/\mu_i)\partial\Psi/\partial r$ at the interface. Then, the confinement energies are determined by the secular equation:

$$\mu_1 k_{yj} K'_{n_j}(k_{yj}) J_{n_j}(k_{xj}) = \mu_2 k_{xj} J'_{n_j}(k_{xj}) K_{n_j}(k_{yj}). \tag{3}$$

The total energies are

$$E_j(k_{xj}, k_{yj}, k_{zj}) = E_{n_j m_j}(k_{xj}, k_{yj}) + E_{zj}(k_{zj}) \qquad E_{zj}(k_{zj}) = \frac{\hbar^2}{2\mu}k_{zj}^2. \tag{4}$$

Finally, u_j is the Bloch function taken at $\vec{k}_0 = 0$, where (by assumption) the band extrema are located.

For an infinitely high potential barrier the wavefunction becomes

$$\Psi_j = [\sqrt{\pi L} r_0 J'_{n_j}(x_{n_j m_j})]^{-1} J_{n_j}\left(x_{n_j m_j}\frac{r}{r_0}\right) \exp(-\mathrm{i}(n_j\phi + k_{zj}z))u_c. \tag{5}$$

Here, $J_{n_j}(x_{n_j m_j} r/r_0)$is the Bessel function of order n_j, $x_{n_j m_j}$ denotes its zeros, $J_{n_j}(x_{n_j m_j}) = 0$ and $J'_{n_j}(x_{n_j m_j})$ is its derivative. On the other hand, the energy levels are determined by

$$E_j = \frac{\hbar^2}{2\mu_j}\left[k_{zj}^2 + \left(\frac{x_{n_j m_j}}{r_0}\right)^2\right]. \tag{6}$$

3. Raman scattering cross section

The DCS for ERS of a volume V per unit solid angle $\mathrm{d}\Omega$ for incoming light of frequency ω_l and scattered light of frequency ω_s is given by [14]

$$\frac{\mathrm{d}^2\sigma}{\mathrm{d}\omega_s\,\mathrm{d}\Omega} = \frac{V^2\omega_s^2\eta(\omega_s)}{8\pi^3 c^4 \eta(\omega_l)} W(\omega_s, \vec{e}_s) \tag{7}$$

where $\eta(\omega)$ is the refractive index as a function of the radiation frequency, $\vec{e}_s$ is the polarization vector for the emitted secondary radiation, c is the velocity of light in vacuum and $W(\omega_s, \vec{e}_s)$ is the transition rate calculated according to

$$W(\omega_s, \vec{e}_s) = \frac{2\pi}{\hbar} \sum_f |M_1 + M_2|^2 \delta(E_f - E_i) \tag{8}$$

where

$$M_j = \sum_{a,b} \frac{\langle f|\hat{H}_{js}|b\rangle\langle b|\hat{H}_{jph}|a\rangle\langle a|\hat{H}_{jl}|i\rangle}{(E_i - E_a + \mathrm{i}\Gamma_a)(E_i - E_b + \mathrm{i}\Gamma_b)} + \sum_{a,c} \frac{\langle f|\hat{H}_{jph}|c\rangle\langle c|\hat{H}_{js}|a\rangle\langle a|\hat{H}_{jl}|i\rangle}{(E_i - E_a + \mathrm{i}\Gamma_a)(E_i - E_c + \mathrm{i}\Gamma_c)}. \tag{9}$$

In equation (9), $|i\rangle$ and $|f\rangle$ denote the initial and final states of the system with their corresponding energies E_i and E_f. $|a\rangle$, $|b\rangle$ and $|c\rangle$ are intermediate states with energies E_a, E_b and E_c while Γ_a, Γ_b and Γ_c are the corresponding lifetime widths. In this equation we have not considered the states related to the 'interference diagrams' [20, 25] because they involve a negligible contribution whenever the energy gap E_g is large enough (as is the case for GaAs, CdTe etc).

The Hamiltonian $\hat{H}_{jl}$ is of the form

$$\hat{H}_{jl} = \frac{|e|}{\mu_0}\sqrt{\frac{2\pi\hbar}{V\omega_l}}\vec{e}_l \cdot \hat{\vec{P}} \qquad \hat{\vec{P}} = -\mathrm{i}\hbar\vec{\nabla} \qquad j = 1, 2 \tag{10}$$

where μ_0 is the free-electron mass. This Hamiltonian describes the interaction with the incident radiation field in the dipole approximation. The interaction with the secondary-radiation field is described by

$$\hat{H}_{js} = \frac{|e|}{\mu_j}\sqrt{\frac{2\pi\hbar}{V\omega_s}}\vec{e}_s \cdot \hat{\vec{P}} \qquad j = 1, 2. \tag{11}$$

This Hamiltonian describes the photon emission by the electron (hole) after transitions between conduction (valence) subbands of the system occur. In equation (9) the intermediate states $|a\rangle$ represent an EHP in a virtual state (after absorption of the incident photon), while the states $|b\rangle$ and $|c\rangle$ represent an EHP in a real one (after the emission of a phonon and a secondary photon, respectively).

In the initial state $|i\rangle$ we have a completely occupied valence band, an unoccupied conduction band and an incident photon of energy $\hbar\omega_l$. Thus,

$$E_i = \hbar\omega_l. \tag{12}$$

The final state $|f\rangle$ involves an EHP excited in a real state, a secondary-radiation emitted photon of energy $\hbar\omega_s$ and a phonon of energy $\hbar\omega_{nm}$. Hence,

$$E_f = E_{n_1m_1} + E_{z_1} + E_{n_2m_2} + E_{z2} + \hbar\omega_s + \hbar\omega_{nm} + E_g. \tag{13}$$

For the intermediate states $|a\rangle$, $|b\rangle$ and $|c\rangle$, the energies E_a, E_b and E_c are easily obtained from the above discussion, and using energy and momentum conservation laws we can evaluate the denominators in equation (9):

$$\begin{aligned} E_i - E_a &= E_{n_1m_1} - E_{n_1''m_1''} + \hbar(\omega_s + \omega_{nm}) \\ E_i - E_b &= E_{n_1m_1} - E_{n_1'm_1'} + \hbar\omega_s \\ E_i - E_c &= E_{n_1m_1} - E_{n_1'm_1'} + \hbar\omega_{nm}. \end{aligned} \tag{14}$$

Considering that the energy of the incident radiation, $\hbar\omega_l$, is such that the electron upon absorbing it could reach the first subbands, and from the above results, the contribution of

the second term of equation (9) can be neglected if it is compared to the contribution of the first one.

We thus should consider, for the determination of the DCS, the contribution of just the first term on the right-hand side of equation (9) during the calculation of M_j.

4. Electron–phonon interaction Hamiltonian

Let us briefly summarize some details concerning the optical phonons and electron–phonon interaction Hamiltonian for QWW and FSW. Within the framework of a macroscopic continuum coupling model, the phonon mechanical displacement vector $\vec{U}$, the electrostatic potential ϕ and the optical vibration modes were obtained in reference [1]. These results are in close agreement with both experiments and microscopic calculations [26–29].

According to this treatment:

(i) we must solve a system of coupled differential equations for the displacement field $\vec{U}$ and the electric potential ϕ;
(ii) we must apply matching conditions at the interfaces in close consistency with both the differential equations of the treatment and the physical principles involved.

This treatment leads to coupled oscillation modes involving a mixed character. For further details, references [26–29] should be consulted.

The boundary conditions that need to be satisfied at the interface are the continuity of:

(1) all the components of the displacement, $\vec{U}$;
(2) the electrostatic potential, ϕ;
(3) the normal component of the mechanical stress tensor, σ_N; and
(4) the normal component of the electric displacement, D_N.

For the GaAs/AlAs system the zone-centre optical phonon frequencies in the two bulk materials are separated by 100 cm^{-1}, which leads to virtually complete confinement of the GaAs vibrations in GaAs and of the AlAs vibrations in AlAs (in fact, the displacements of GaAs modes are zero at the first Al atom after the interface). In order to simplify the algebra, the boundary condition (1) is modified from $\vec{U}$ continuous to $\vec{U} = 0$ at the interface. With this modification, the stress boundary condition (3) becomes redundant.

Other cases also considered in the literature are free oscillations for FSW. In such cases the active medium is surrounded by vacuum (or quartz), thus allowing free oscillations of the surface. In this case the matching boundary conditions are $\overleftrightarrow{\sigma}\vec{N}|_{r\in S} = 0$ and $\vec{U}$ is defined for just one side of the structure.

In the framework of the present treatment we shall restrict ourselves to the case of oscillations perpendicular to the wire axis, i.e., $q_z = 0$ and hence $U_z = 0$, where $\vec{q}$ is the phonon wavevector. We are thus considering a particular case which, however, is of direct relevance to the study of certain physical outcomes (one-phonon Raman scattering configurations [30], for instance) and gives us an insight into the nature of the oscillations. It has been shown that the corresponding eigensolutions constitute a complete orthonormal basis of eigenvectors $\vec{U}_{nm}$ and the electron–phonon interaction Hamiltonian is derived using the second-quantization formalism and can be written as [1]

$$\hat{H} = \sum_{n,m} C_{nm}[F_{nm}(r)\mathrm{e}^{\mathrm{i}n\theta}\hat{b}_{nm} + \mathrm{HC}] \tag{15}$$

where

$$C_{nm} = \left[\frac{\pi\omega_L\rho}{\omega_{nm}}\right]^{1/2} r_0^2 C_F \qquad C_F = -\sqrt{\frac{2\pi e^2\hbar\omega_L}{V}(\epsilon_{a\infty}^{-1} - \epsilon_{a0}^{-1})}. \tag{16}$$

$\epsilon_{a\infty}$ (ϵ_{b0}) is the high-frequency (static) dielectric constant; V is the volume; ω_L is the limiting (bulk) longitudinal optical frequency of the oscillations; ρ is the reduced mass density; ω_{nm} is the frequency of the nm-mode; the functions $F_{nm}(r)$ have different forms for the QWW and FSW. For a QWW, we have that

$$F_{nm}^{QWW} = B_{nm} \begin{cases} \dfrac{1}{x} f_n\left(x\dfrac{r}{r_0}\right) - S_n(x)\left(\dfrac{r}{r_0}\right)^n & r < r_0 \\ \left[\dfrac{1}{x} f_n(x) - S_n(x)\right]\left(\dfrac{r_0}{r}\right)^n & r > r_0 \end{cases} \tag{17}$$

where

$$S_n(x) = \frac{\epsilon_{a\infty}}{\epsilon_{a\infty} + \epsilon_{b\infty}}\left[\frac{1}{n} f_{n-1}(x) + \frac{1}{x}\left(\frac{\epsilon_{b\infty} - \epsilon_{a\infty}}{\epsilon_{a\infty}}\right) f_n(x)\right] \tag{18}$$

while for a FSW

$$F_{nm}^{FSW} = B_{nm} \begin{cases} f_n\left(x\dfrac{r}{r_0}\right) - t_n(x, y)\left(\dfrac{r}{r_0}\right)^n & r < r_0 \\ [f_n(x) - t_n(x, y)]\left(\dfrac{r_0}{r}\right)^n & r > r_0 \end{cases} \tag{19}$$

where

$$t_n(x, y) = \left[y^2 f_n(x) f_{n+2}(y) + \frac{\epsilon_{a\infty}}{\epsilon_{b\infty}} g_n(x) f_n(y)\right]\left[\left(\frac{\epsilon_{a\infty}}{\epsilon_{b\infty}}\left(\frac{\beta_L}{\beta_T}\right)^2 x^2 + y^2\right) f_{n+2}(y)\right]^{-1} \tag{20}$$

and

$$g_n(x) = \frac{\beta_L^2}{\beta_T^2} x^2 f_n(x) - 2(n+1) x f_{n+1}(x). \tag{21}$$

B_{nm} is a normalization constant which can be determined from equation (34) in [1]. In this constant we may include the term ρ from equation (16); therefore it will not appear later. $\epsilon_{b\infty}$ is the high-frequency dielectric constant for AlAs. β_L (β_T) is a parameter describing the dispersion of the longitudinal (transverse) oscillations.

On the other hand,

$$x = q r_0 \qquad y = Q r_0 \qquad \left(\frac{r_0}{\beta_L}\right)^2 (\omega_L^2 - \omega_T^2) = R^2 = x^2 - \left(\frac{\beta_T}{\beta_L}\right)^2 y^2 \tag{22}$$

where

$$q^2 = \frac{\omega_L^2 - \omega_{nm}^2}{\beta_L^2} \qquad Q^2 = \frac{\omega_T^2 - \omega_{nm}^2}{\beta_T^2}$$

and $f_n(x)$ represents a solution of the Bessel equation of order n (this function should be bounded in its domain of definition). It must be noted that $\omega < \omega_L$ for all of the frequencies involved; thus q is always a real quantity. In contrast, Q is real for $\omega < \omega_T$, but a pure complex quantity for $\omega_T < \omega < \omega_L$.

The eigenfrequencies of the oscillation modes for this case are reported in [4] as

$$\frac{\epsilon_{a\infty} + \epsilon_{b\infty}}{2}[f_{n-1}(x) f_{n+1}(y) + f_{n-1}(y) f_{n+1}(x)] + \left(\frac{\beta_L}{\beta_T}\right)^2 \frac{\epsilon_{a\infty}}{y^2} R^2\left[f_{n-1}(x) + \frac{n}{x} f_n(x)\left(\frac{\epsilon_{b\infty}}{\epsilon_{a\infty}} - 1\right)\right] f_{n+1}(y) = 0 \tag{23}$$

and for the FSW case they are obtained by solving the following secular equation:

$$2n(n-1)\left(\frac{\beta_L}{\beta_T}\right)^2 R^2 t_n(x, y) f_{n+2}(y) + 2n y^2 f_{n+2}(y)[x f_n'(x) - f_n(x)] + g_n(x)[2y f_n'(y) + (y^2 - 2n^2) f_n(y)] = 0. \tag{24}$$

5. Calculation of Raman scattering intensities in QWW

If we consider allowed electron transitions between conduction (c) and valence (v) bands, equations (10) and (1), the matrix element $\langle a|\hat{H}_{jl}|i\rangle$, in the envelope function approximation, can be written as

$$\langle a|\hat{H}_{jl}|i\rangle = \frac{|e|}{\mu_0}\sqrt{\frac{2\pi\hbar}{V\omega_l}}\vec{e}_l \cdot \hat{\vec{P}}_{cv}(0) \begin{cases} \chi_{n_2m_2}^{n_1''m_1''}\delta_{n_1''n_2}\delta_{k_1'',-k_2} & j=1 \\ \chi_{n_1m_1}^{n_2''m_2''}\delta_{n_1n_2''}\delta_{k_1,-k_2''} & j=2 \end{cases} \tag{25}$$

with

$$\chi_{n_2m_2}^{n_1m_1} = A_{n_1m_1}A_{n_2m_2}\int_0^{r_0} J_{n_1}(x_{n_1m_1})J_{n_2}(x_{n_2m_2})r\,\mathrm{d}r + B_{n_1m_1}B_{n_2m_2}\int_{r_0}^{\infty} K_{n_1}(y_{n_1m_1})K_{n_2}(y_{n_2m_2})r\,\mathrm{d}r \tag{26}$$

where $\hat{\vec{P}}_{cv}$ is the momentum matrix connecting the valence and conduction bands (evaluated at $\vec{k}_0 = 0$).

From equations (15)–(18) and equation (1) it can be seen that

$$\langle b|\hat{H}_{jph}|a\rangle = C_{nm}I_{n_j''m_j''n}^{n_j'm_j'm}\delta_{n_j'',n_j'-n}\delta_{k_j'',k_j'} \tag{27}$$

where

$$I_{n_j''m_j''n}^{n_j'm_j'm} = A_{n_j'm_j'}A_{n_j''m_j''}\int_0^{r_0} J_{n_j'}(x_{n_j'm_j'})F_{nm}^{QWW}(r)J_{n_j''}(x_{n_j''m_j''})r\,\mathrm{d}r + B_{n_j'm_j'}B_{n_j''m_j''}\int_{r_0}^{\infty} K_{n_j'}(y_{n_j'm_j'})F_{nm}^{QWW}(r)K_{n_j''}(y_{n_j''m_j''})r\,\mathrm{d}r. \tag{28}$$

For the electron (hole)–secondary-radiation interaction matrix element we have

$$\langle f|\hat{H}_{js}|bj\rangle = (-1)^{j+2}\frac{|e|\mathrm{i}\hbar}{\mu_j}\sqrt{\frac{2\pi\hbar}{V\omega_l}}\vec{e}_s \cdot \vec{\nabla}_{jj}$$

where

$$\nabla_{jj} = \left\{\frac{\sqrt{2}}{2}[(x_{n_j,m_j'}J_{n_j,m_jm_j'} - y_{n_j,m_j'}K_{n_j,m_jm_j'})\hat{\tilde{\sigma}}_{-}\delta_{n_j,n_j'-1} - (x_{n_j,m_j'}J_{n_j,m_jm_j'} + y_{n_j,m_j'}K_{n_j,m_jm_j'})\hat{\tilde{\sigma}}_{+}\delta_{n_j,n_j'+1}] - \mathrm{i}k_j'(J_{n_j,m_jm_j'} + K_{n_j,m_jm_j'})\hat{\tilde{Z}}\delta_{n_j,n_j'}\right\}\delta_{k_j,k_j'} \tag{29}$$

$$J_{n_j,m_jm_j'} = A_{n_j,m_j}A_{n_j,m_j'}\int_0^{r_0} J_{n_j}(x_{n_jm_j})J_n(x_{n_jm_j'})r\,\mathrm{d}r \tag{30}$$

$$K_{n_j,m_jm_j'} = B_{n_j,m_j}B_{n_j,m_j'}\int_{r_0}^{\infty} K_{n_j}(y_{n_jm_j})K_{n_j}(y_{n_jm_j'})r\,\mathrm{d}r. \tag{31}$$

Using the theory described in section 2 we can obtain, after cumbersome calculations, explicit expressions for the DCS of the ERS process. We have neglected the photon wavevector in comparison with the electron wavevector in our calculation. Hence, in the final state, we have $\vec{k}_e + \vec{k}_h = 0$. We just write the final results:

$$\frac{\mathrm{d}^2\sigma}{\mathrm{d}\Omega\,\mathrm{d}\omega_s} = \sigma_0[W_{e_{sz}} + W_{e_s^+} + W_{e_s^-} + W_{e_s^+e_s^-}] \tag{32}$$

where

$$\sigma_0 = \frac{2\sqrt{2}e^6|\vec{e}_l \cdot \widehat{\vec{P}}_{cv}|^2\eta(\omega_s)\omega_L\omega_s\hbar^4}{\mu_r^2 E_0^5\mu_0^2c^4\eta(\omega_l)\omega_l r_0^3}(\epsilon_\infty^{-1} - \epsilon_0^{-1}) \tag{33}$$

$$W_{e_{sz}} = \sum_{n_1m_1n_2m_2nm} \frac{\omega_{LO}}{\omega_{nm}} \left|M_{e_{sz}}\right|^2 \sqrt{g^2 + \sqrt{g^4+\delta^2}} \left|\vec{e}_s \cdot \widehat{\vec{Z}}\right|^2 \tag{34}$$

$$W_{e_s^\mp} = \sum_{n_1m_1n_2m_2nm} \frac{\omega_{LO}}{\omega_{nm}} \left|M_{e_s^\mp}\right|^2 \sqrt{\frac{g^2 + \sqrt{g^4+\delta^2}}{g^4+\delta^2}} |\vec{e}_s \cdot \vec{\sigma}_\mp|^2 \tag{35}$$

and

$$W_{e_s^+e_s^-} = -2 \sum_{n_1m_1n_2m_2nm} \frac{\omega_{LO}}{\omega_{nm}} (\mathrm{Re}\, M_{e_s^-}\, \mathrm{Re}\, M_{e_s^+} + \mathrm{Im}\, M_{e_s^-}\, \mathrm{Im}\, M_{e_s^+}) \times \sqrt{\frac{g^2 + \sqrt{g^4+\delta^2}}{g^4+\delta^2}} \delta_{n0}(\vec{e}_s \cdot \vec{\sigma}_-)(\vec{e}_s \cdot \vec{\sigma}_+) \tag{36}$$

where

$$M_{e_{sz}} = \sum_{j=1}^{2} \sum_{m_j''m_j'} \frac{(J_{n_j,m_jm_j'} + K_{n_j,m_jm_j'})}{[E_{bj} + \mathrm{i}\delta_{bj}][E_a(n_j, m_j, n_2\delta_{1j} + n_1\delta_{2j}, m_j'') + \mathrm{i}\delta_{aj}]} \times (I^{n_1m_1'm}_{n_2m_1''n}\, \chi^{n_2m_1''}_{n_2m_2}\delta_{n_2,n_1-n}\delta_{1j} + I^{n_2m_2'm}_{n_1m_2''n}\, \chi^{n_1m_2''}_{n_1m_1}\delta_{n_1,n_2-n}\delta_{2j})\delta_{n_j',n_j} \tag{37}$$

$$M_{e_s^\mp} = \frac{\sqrt{2}}{2} \sum_{j=1}^{2} \sum_{m_j''m_j'} \frac{(-1)^{j+1}(x_{n_j,m_j'}J_{n_j,m_jm_j'} \mp y_{n_j,m_j'}K_{n_j,m_jm_j'})}{[E_{bj} + \mathrm{i}\delta_{bj}][E_a(n_j, m_j, n_2\delta_{1j} + n_1\delta_{2j}, m_j'') + \mathrm{i}\delta_{aj}]} \times (I^{n_1'm_1'm}_{n_2m_1''n}\, \chi^{n_2m_1''}_{n_2m_2}\delta_{n_2,n_1\pm1-n}\delta_{1j} + I^{n_2'm_2'm}_{n_1m_2''n}\, \chi^{n_1m_2''}_{n_1m_1}\delta_{n_1,n_2\pm1-n}\delta_{2j})\delta_{n_j',n_j\pm1} \tag{38}$$

where

$$E_a(n_j, m_j, n_2\delta_{1j} + n_1\delta_{2j}, m_j'') = \frac{1}{E_0}[\hbar\omega_s + \hbar\omega_{nm} + E^{(j)}_{n_jm_j} - E^{(j)}_{n_2\delta_{1j}+n_1\delta_{2j},m_j''}] \tag{39}$$

$$E_{bj} = \frac{1}{E_0}[E^{(j)}_{n_jm_j} - E^{(j)}_{n_j'm_j'} + \hbar\omega_s] \tag{40}$$

$$g^2 = \frac{1}{E_0}[\hbar\omega_l - \hbar\omega_s - \hbar\omega_{nm} - E_g - E_{n_1m_1} - E_{n_2m_2}] \tag{41}$$

$$E_0 = \frac{\hbar^2}{2\mu_r r_0^2} \qquad \mu_r^{-1} = \mu_e^{-1} + \mu_h^{-1} \tag{42}$$

where μ_e and μ_h are the electron and hole effective masses within the QWW.

Derivation of equations (32), (34), (35) and (36) requires that

$$\delta(E_f - E_i) \to \frac{1}{\pi}\frac{\Gamma_f}{(E_f - E_i)^2 + \Gamma_f^2} \tag{43}$$

assuming a finite lifetime for the EHP in the final state, while

$$\delta_f = \frac{\Gamma_f}{E_0} \qquad \delta_a = \frac{\Gamma_a}{E_0} \qquad \delta_b = \frac{\Gamma_b}{E_0}. \tag{44}$$

In equation (32) four terms can be observed, in contrast with the case for equation (10) of [13] where only the first three exist; the last term is related to the confined phonons and only has meaning for $n = 0$ where LO and TO phonon modes are uncoupled (see equation (36)).

Let us make some remarks concerning the above equations. For a general scattering configuration we should have four terms in the DCS, as is explicitly seen in equation (32). However, for particular choices of the scattering configuration some of these terms could be absent. For instance, if we have a backscattering configuration with $\vec{Z}$ parallel to the radiation wavevector $\vec{k}$, then equation (34) will not contribute to the DCS. In particular, for the scattering configuration $\bar{Z}(\vec{e}_l, \vec{\sigma}_\pm)Z$, the contribution to the DCS is given by (35) and (36). In the configuration where the scattered radiation wavevector is parallel to the x-axis with polarization $\vec{e}_s \| \vec{Z}$, i.e., $\bar{Z}(\vec{e}_l, Z)X$, only the first term on the right-hand side of equation (32) will be present in the DCS. This result is in close analogy with the case of ERS in cylindrical quantum wires [13]. In equations (34), (35) and (36) the summations over the labels $(n_1, m_1, n_2, m_2, n, m)$ must be carried out obeying the following requirement:

$$\frac{1}{E_0}[\hbar\omega_l - \hbar\omega_s - \hbar\omega_{nm} - E_g - E_{n_1m_1} - E_{n_2m_2}] \geqslant 0. \tag{45}$$

In the $\bar{Z}(\vec{e}_l, \vec{\sigma}_\pm)Z$ configuration the emission spectra of ERS in QWW show maxima at the following values of ω_s:

$$\omega_s^j = \frac{1}{\hbar}[E^{(j)}_{n_2\delta_{1j}+n_1\delta_{2j},m_j''} - E^{(j)}_{n_jm_j} - \hbar\omega_{nm}] \tag{46}$$

and

$$\omega_s^j = \frac{1}{\hbar}[E^{(j)}_{n_j'm_j'} - E^{(j)}_{n_jm_j}]. \tag{47}$$

As can be seen from equation (46) or (47), these frequencies correspond to electron transitions connecting the subband edges for a process involving just the conduction or just the valence band (i.e., intraband transitions). The values of frequencies reported in equations (46) and (47) are associated with the emission of a phonon (photon) by the electron or hole in intersubband transitions. The selection rules are $n_2 = n_1 \pm 1 - n$ for the electron transitions and $n_2 = n_1 \mp 1 + n$ for the hole transitions, both related to equation (46). We also observe in equation (47) that for $n_1' = n_1 \pm 1$ ($n_2' = n_2 \pm 1$), electron (hole) transitions are allowed. This selection rule corresponds to $e_s^{\mp}$-polarization. The singularities involved in equations (46) and (47) are independent of ω_l and correspond to intraband transitions.

Other singularities of equations (35) and (36) occur whenever $g = 0$. Such singularities are mainly related to certain values of the frequency ω_l of the incident photon. For the emission spectra the positions of these singularities are given as follows:

$$\omega_s = \frac{1}{\hbar}[\hbar\omega_l - \hbar\omega_s - \hbar\omega_{nm} - E_g - E_{n_1m_1} - E_{n_2m_2}]. \tag{48}$$

Here the same selection rule as applies to equation (46) must be fulfilled. The peaks related to the latter singularities correspond to interband EHP transitions and their positions depend on the incident radiation frequency ω_l.

In the case of the scattering configuration $\bar{Z}(\vec{e}_l, \vec{e}_{sz})X$, the following selection rules are satisfied: $n_2 = n_1 - n$ for electron transitions while $n_2 = n_1 + n$ for the hole transitions. In this case, the emission spectra of the ERS show maxima for the values of ω_s given in (46). If the transitions are mediated by photons, the selection rules are given by $n_2 = n_1$.

6. Calculation of the Raman scattering intensities in FSW

If we consider allowed electron transitions between conduction (c) and valence (v) bands, equations (5) and (10), the matrix element $\langle a|\hat{H}_{jl}|i\rangle$, in the envelope function approximation,

can be written as

$$\langle a|\hat{H}_{jl}|i\rangle = \frac{|e|}{\mu_0}\sqrt{\frac{2\pi\hbar}{V\omega_l}}\vec{e}_l \cdot \widehat{\vec{P}}_{cv}(0)\begin{cases}\delta_{n_1''n_2}\delta_{m_1''m_2}\delta_{k_1',-k_2} & j=1\\ \delta_{n_1n_2''}\delta_{m_1m_2''}\delta_{k_1,-k_2''} & j=2.\end{cases} \tag{49}$$

From equations (5) and (15) it can be seen that

$$\langle b|\hat{H}_{jph}|a\rangle = C_{nm}I^{n_j'm_j'm}_{n_j''m_j''n}\left[\frac{r_0^2}{2}J'_{n_j'}(x_{n_j'm_j'})J'_{n_j''}(x_{n_j''m_j''})\right]^{-1}\delta_{n_j'',n_j'-n}\delta_{k_j'',k_j'} \tag{50}$$

where

$$I^{n_j'm_j'm}_{n_j''m_j''n} = \frac{1}{r_0}\int_0^{r_0} J_{n_j'}\left(x_{n_j'm_j'}\frac{r}{r_0}\right)F^{FSW}_{nm}(r)J_{n_j''}\left(x_{n_j'm_j'}\frac{r}{r_0}\right)r\ \mathrm{d}r. \tag{51}$$

For the electron (hole)–secondary-radiation interaction matrix element, we have

$$\langle f|\hat{H}_{js}|b\rangle = \frac{\mathrm{i}\hbar e}{\mu_j}\sqrt{\frac{2\pi\hbar}{V\omega_s}}(-1)^{j+1}\{\mathrm{i}k_j'\vec{e}_s\cdot\vec{Z}\delta_{n_jn_j'}\delta_{m_jm_j'} - \frac{\vec{e}_s\cdot\vec{\sigma}_-}{r_0}Y^+_{n_jm_jm_j'}\delta_{n_j',n_j+1} - \frac{\vec{e}_s\cdot\vec{\sigma}_+}{r_0}Y^-_{n_jm_jm_j'}\delta_{n_j',n_j-1}\}\delta_{k_jk_j'} \tag{52}$$

where

$$Y^{\pm}_{nlm} = \frac{x_{n\pm1,m}x_{nl}}{(x_{nl})^2-(x_{n\pm1,m})^2} \qquad \text{and} \qquad \vec{\sigma}_\pm = (\vec{X}\pm\mathrm{i}\vec{Y}). \tag{53}$$

We just obtain the final results in a similar way to equations (32), (33), (35) and (36), but

$$W_{e_{sz}} = \sum_{\substack{n_1m_1n_2\\ m_2nm}}\left\{\frac{\omega_L}{\omega_{nm}}\left(\frac{I^{n_1m_1m}_{n_2m_2n}}{J(n_1m_1n_2m_2)}\right)^2 \times \frac{\sqrt{g^2+\sqrt{g^4+\delta_f^2}}}{(\hbar\omega_s/E_0)^2+\delta_b^2}\left|\frac{\beta_1\delta_{n_2,n_1-n}}{p_{1a}+\mathrm{i}\delta_a}+\frac{\beta_2\delta_{n_2,n_1+n}}{p_{2a}+\mathrm{i}\delta_a}\right|^2\right\}\left|\vec{e}_s\cdot\vec{Z}\right|^2 \tag{54}$$

$$M_{e_s^{\mp}} = \sum_{j=1}^{2}\left\{(-1)^j\sum_{n_j'm_j'}\frac{\beta_jI_jY^{\pm}_{n_jm_jm_j'}\delta_{n_j',n_j\pm1}}{J_j(p_{jb}+\mathrm{i}\delta_b)}\frac{\delta_{1j}\delta_{n_2,-n+n_1\pm1}+\delta_{2j}\delta_{n_2,n+n_1\mp1}}{(p_{ja}+\mathrm{i}\delta_a)}\right\} \tag{55}$$

where

$$I_1 = I^{n_1'm_1'm}_{n_2m_2n} \qquad I_2 = I^{n_2'm_2'm}_{n_1m_1n} \qquad J_1 = J(n_1'm_1'n_2m_2) \qquad J_2 = J(n_1m_1n_2'm_2') \tag{56}$$

and

$$J(n_1m_1n_2m_2) = J'_{n_1}(\mu^{n_1}_{m_1})J'_{n_2}(\mu^{n_2}_{m_2}). \tag{57}$$

On the other hand,

$$p_{ja} = (-1)^{j+1}\beta_j[(x_{n_1m_1})^2-(\mu_{n_2m_2})^2]+\frac{\hbar(\omega_s+\omega_{nm})}{E_0} \tag{58}$$

$$p_{jb} = \beta_j[(\mu_{n_jm_j})^2-(\mu_{n_j'm_j'})^2]+\frac{\hbar\omega_s}{E_0} \tag{59}$$

with

$$g^2 = \frac{1}{E_0}(\hbar\omega_l-\hbar\omega_s-\hbar\omega_{nm}-E_g)-\beta_1(x_{n_1m_1})^2-\beta_2(x_{n_2m_2})^2 \tag{60}$$

assuming a finite lifetime for the EHP in the final state, while

$$\beta_j = \frac{\mu_r}{\mu_j}. \tag{61}$$

In the $\bar{Z}(\vec{e}_l, \vec{\sigma}_\pm)Z$ configuration, the emission spectra of the ERS in QWW show maxima at the following values of ω_s:

$$\omega_s^j = (-1)^{j+1}\frac{\beta_j E_0}{\hbar}[(x_{n_2m_2})^2 - (x_{n_1m_1})^2] - \omega_{nm} \tag{62}$$

and

$$\omega_s^j = \frac{\beta_j E_0}{\hbar}[(x_{n'_jm'_j})^2 - (x_{n_jm_j})^2]. \tag{63}$$

The selection rules are similar to those in the QWW case, except the $n_2 = n_1$ one for the $\bar{Z}(\vec{e}_l, Z)X$ scattering configuration.

Other singularities occur whenever $g = 0$. For the emission spectra the positions of these singularities are given as follows:

$$\omega_s(n_1, m_1, m_2, n, m) = \omega_l - \omega_{nm} - \omega_g - \frac{\beta_1 E_0}{\hbar}(x_{n_1m_1})^2 - \frac{\beta_2 E_0}{\hbar}(x_{n_2m_2})^2. \tag{64}$$

The peaks related to the latter singularities correspond to interband EHP transitions and their positions depend on the incident radiation frequency ω_l.

7. Discussion of the results and conclusions

We have computed the scattering efficiency (SE) $(1/\sigma_0)\mathrm{d}^2\sigma/\mathrm{d}\Omega\,\mathrm{d}\omega_s$ as a function of $\hbar\omega_s/E_0$ and $(1/\sigma_0)\mathrm{d}^2\sigma/\mathrm{d}\Omega\,\mathrm{d}\omega_s$ as a function of $(\hbar\omega_l - E_g)/E_0$—the so-called 'emission and excitation spectra', respectively—for the ERS process for a given polarization $\vec{e}_s$ of the emitted radiation. The physical parameters used in our expressions are: for the GaAs case, $E_g = 1.5177$ eV, $\mu_1 = 0.0665\mu_0$, $\mu_2 = 0.45\mu_0$ (the heavy-hole band), $\epsilon_\infty = 10.9$, $\epsilon_0 = 12.53$, $\beta_T = 3.12 \times 10^{-12}$, $\beta_L = 2.91 \times 10^{-12}$, $\omega_T = 273.8$ cm^{-1}; and for the AsAl case, $\mu_1 = 0.12\mu_0$, $\mu_2 = 0.5\mu_0$, $\epsilon_\infty = 8.16$, $\epsilon_0 = 10.06$. We have set $\Gamma_f = 3$ meV, $\Gamma_a = \Gamma_b = 1$ meV, $V_e = 0.968$ eV and $V_h = 0.6453$ eV.

Resonant electron transitions mediated by photons (phonons) are indicated by $\omega_{e,s}(n_1, m_1, n'_1, m'_1)$ ($\omega_{e,ph}(n_1, m_1, n_2, m_2)$). In the hole case we have $\omega_{h,s}(n'_2, m'_2, n_2, m_2)$ ($\omega_{h,ph}(n_1, m_1, n_2, m_2)$). Here, (n_a, m_a, n_b, m_b) represents the subband involved in the transitions. The step-like ones are indicated by $\mathrm{SL}(n_1, m_1, n_2, m_2)$, where n_1 and m_1 (n_2 and m_2) are the electron (hole) subbands.

In figure 1(a) we show the emission spectra of the QWW in the scattering configuration $\overline{Z}(\vec{e}_l, \vec{\sigma}_-)Z$. We have selected the following values: $\hbar\omega_l - E_g = 20E_0$ (dotted line), $\hbar\omega_l - E_g = 25E_0$ (solid line), $r_0 = 2$ nm and $n_{ph} = 0$. It can be observed that the positions of the peaks, which appear due to photon and phonon emission, do not depend on the incident energy, but they do depend on the difference of the subbands that appear to be involved in the transitions and also on the phonon mode when the phonon is involved (see equations (46) and (47)). On the other hand, the increase of the incident energy produces a decrease of the DCS (see equations (35) and (41)).

Figure 1(b) shows the emission spectra for a QWW with the same scattering configuration as was used in figure 1(a). The selected values are: $r_0 = 2$ nm, $\hbar\omega_l - E_g = 20E_0$ for $n_{ph} = 0$ (solid line) and $n_{ph} = 1$ (dotted line). It can be observed that the positions of the peaks due to transitions assisted by photon emission do not depend on the phonon mode that is involved; however, their intensity increases with the phonon mode, since the DCS is inversely

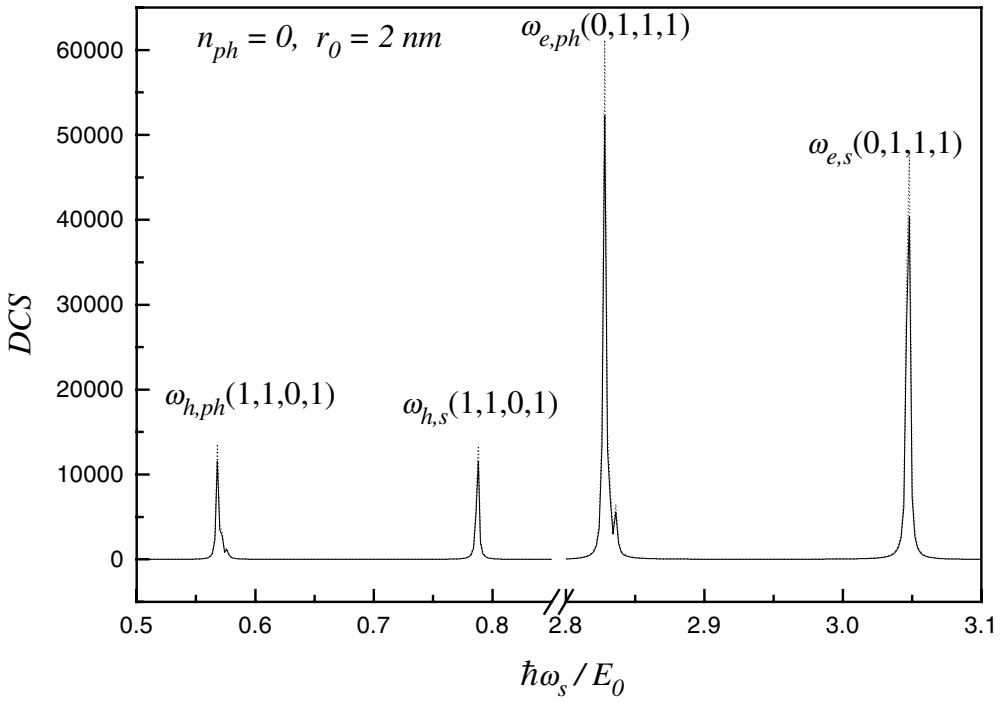

(a)

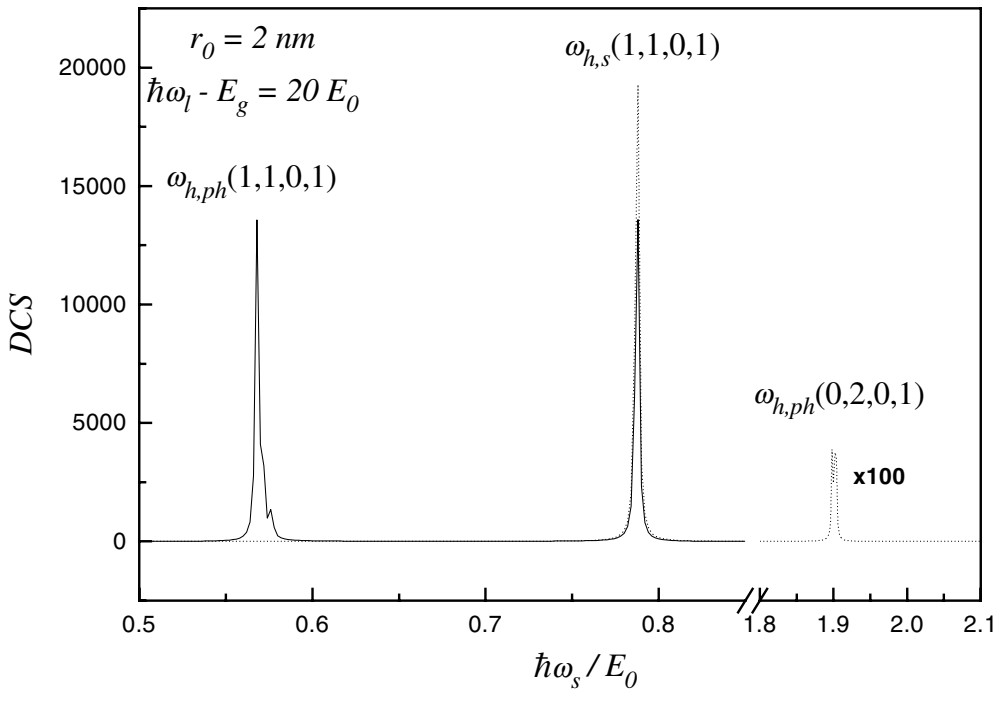

(b)

Figure 1. Emission spectra of the QWW in the $\overline{Z}(\vec{e}_l, \vec{\sigma}_-)Z$ scattering configuration for: (a) $\hbar\omega_l - E_g = 20E_0$ (dotted line), $\hbar\omega_l - E_g = 25E_0$ (solid line) and (b) $\hbar\omega_l - E_g = 20E_0$, $n_{ph} = 0$ (solid line) and $n_{ph} = 1$ (dotted line).

proportional to its frequency (see the dispersion relation given in [1] and equation (35)). The presence of a finite potential barrier can produce a different behaviour of the higher-order phonon modes because the selection rules impose the requirement that the transitions take place between more separated subbands, resulting in an energy separation higher than the energy of the vibration modes. If the potential barrier is infinite, the inverse dependency on the mode frequency is always retained.

Figure 2 shows the emission spectra of a QWW in the scattering configuration $Z(\vec{e}_l, Z)X$ for two values of the incident energies: $\hbar\omega_l - E_g = 20E_0$ (solid line) and $\hbar\omega_l - E_g = 31E_0$ (dotted line). Both spectra correspond to the modes $n_{ph} = 0$ and $r_0 = 2$ nm. The increase of the incident energy produces a behaviour similar to the one discussed previously. In this case, in contrast to that in reference [13], the singular character appears in the spectrum for two reasons:

(1) the consideration of transitions in which the phonons participating have oscillations perpendicular to the z-axis ($q_z = 0$); and
(2) the presence of the finite potential barrier, which leads to the indices m_1 and m_2 of the electron and hole subbands not being coupled.

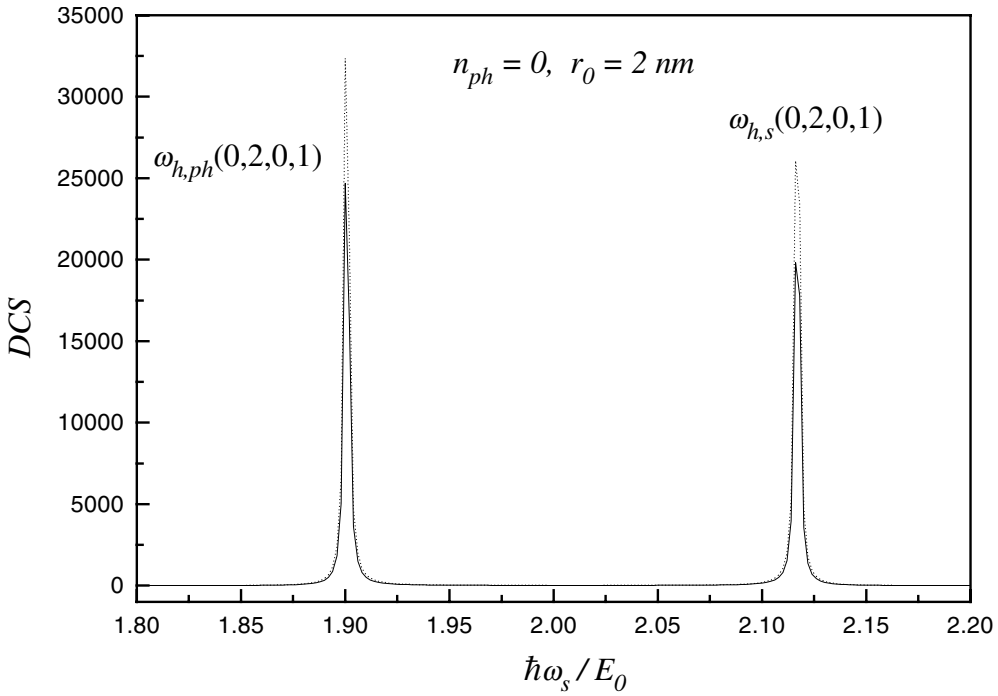

Figure 2. Emission spectra of the QWW in the $Z(\vec{e}_l, Z)X$ scattering configuration. $\hbar\omega_l - E_g = 20E_0$ (solid line) and $\hbar\omega_l - E_g = 31E_0$ (dotted line).

In figure 3 we show the emission spectrum for several values of the potential barrier for electrons, using the same scattering configuration and data as in figure 1(a). In these spectra the values of the potential barrier in the valence band and the effective masses of electrons and holes have been fixed. It can be observed that for a particular transition, the position of the peaks is shifted to the right when the value of the potential barrier of the conduction band increases. This shows that the position of the peaks is affected by the presence of the finite

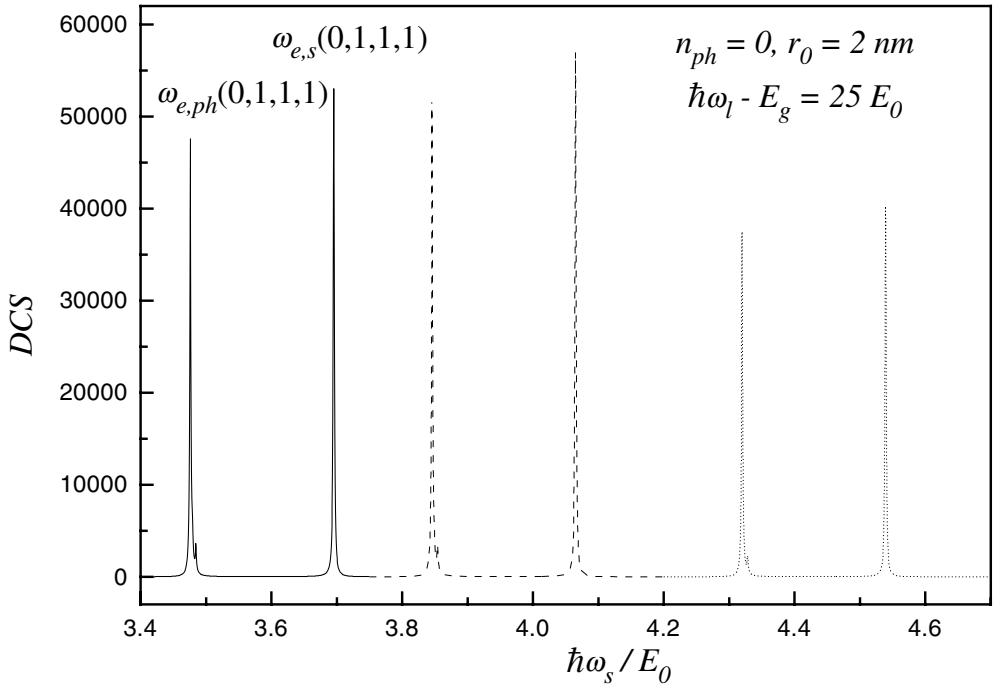

Figure 3. Emission spectra of the QWW in the $\overline{Z}(\vec{e}_l, \vec{\sigma}_-)Z$ scattering configuration. Solid line: 1.5 eV; dashed line: 2 eV; dotted line: 3 eV.

barrier, and we can observe that for the infinite potential barrier, the position of the peaks would be the limit case.

In figure 4 we show the emission spectra of the FSW in the scattering configuration $Z(\vec{e}_l, Z)X$ with $\hbar\omega_l - E_g = 20E_0$. We must point out that the spectra are plotted keeping in mind that the electron and hole are completely confined. This allows one to invoke an analogy with the case of the QWW modelled with infinite potential barriers since the system of electrons and holes would be in the same situation in the two cases; the only difference would be in the phonon system due to the fact that for the QWW the boundary conditions are of the first type while for the FSW they are of the second type. Keeping in mind the dispersion relations given in reference [1], and equation (62), it can be observed that the position of the peaks would be slightly shifted to the right in the case of the FSW. On the other hand, the magnitude of the DCS for the FSW is much larger than for the QWW, which is possible because the boundary conditions lead to the form factor of the FSW being much larger than for the QWW. If the QWW is modelled with a finite barrier, then the shifting would not be small; in fact the position of the peaks would be shifted to the left and another transition would appear (according to the discussion of figure 3). That behaviour can be observed for all possible peaks.

In figure 4 it can also be observed that the only transitions appearing are those in which phonons are emitted. The behaviour is different in the case where the potential barrier is finite, where, besides this transition, other transitions appear, which are due to photons (see figure 2). On the other hand, upon comparing the positions of the peaks having the same phonon mode but with different radius, one can observe a shift to the left when the radius increases.

Figure 5 shows the excitation spectra of a QWW with the scattering configuration of figure 2. Here $n_{ph} = 0$, $r_0 = 2$ nm and $\hbar\omega_s = 6E_0$. It can be observed that new subbands are

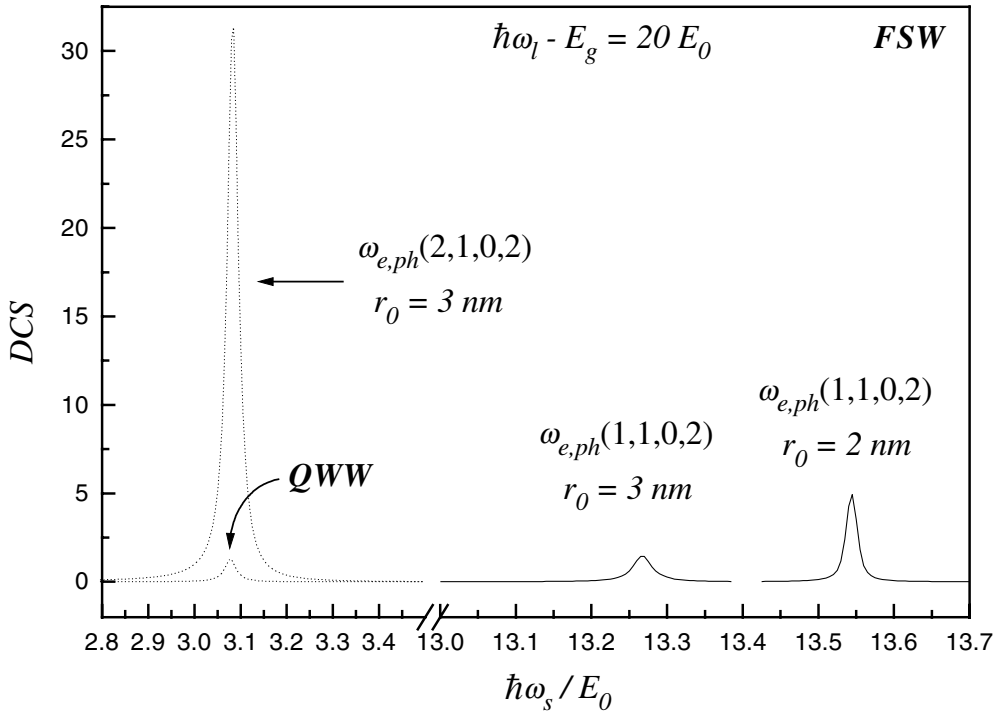

Figure 4. Emission spectra of the FSW in the $Z(\vec{e}_l, Z)X$ scattering configuration. Solid line: $n_{ph} = 1$; dotted line: $n_{ph} = 0$.

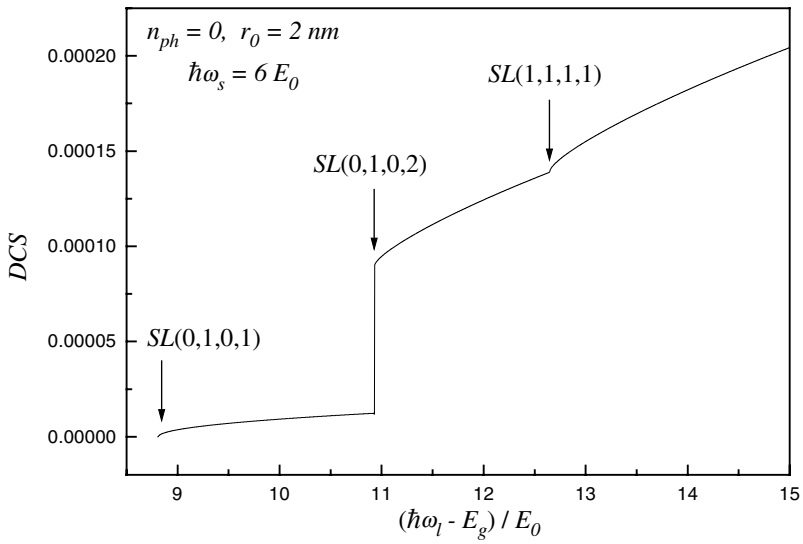

Figure 5. The excitation spectrum of the QWW in the $Z(\vec{e}_l, Z)X$ scattering configuration.

accessible to the EHP when the incident energy is increased. The effect of the finite barrier in the spectrum is observed in the transition SL(0, 1, 0, 2).

Finally, in the present work we have applied a simplified model for the electronic structure

of the system. In a more realistic case we should consider a coupled band structure using a calculation model like that of Luttinger and Kohn or the Kane model. The above-mentioned assumptions would lead to better results but entail more complicated calculations. However, within the limits of our simple model we are able to account for the essential physical properties of the problem discussed. The fundamental features of the DCS, as described in this work, should not be very different in the real QWW case. It can be easily proved that the singular peaks in the DCS will be present irrespective of the model used for the subband structure and may be determined for values of $\hbar\omega_s$ equal to the energy difference between two subbands: $\hbar\omega_s^{e\,(h)} = E_\alpha^{e\,(h)} - E_\beta^{e\,(h)}$, where $E_\alpha^{e\,(h)}$ ($E_\beta^{e\,(h)}$) are the respective electron (hole) energies in the subbands. Similarly, we shall have a step-like dependence in the DCS for $\hbar\omega_l = \hbar\omega_s + \hbar\omega_{nm} + E_g + E_\alpha + E_\beta$. At present there is a lack of experimental work on this type of ERS. Our major aim in performing these calculations is to stimulate experimental research in this direction.

References

[1] Comas F, Cantarero A, Trallero-Giner C and Moshinsky M 1995 *J. Phys.: Condens. Matter* **7** 1789
[2] Trallero-Giner C 1994 *Physica* T **55** 50
[3] Trallero-Giner C and Comas F 1994 *Phil. Mag.* B **70** 583
[4] Comas F, Trallero-Giner C and Cantarero A 1993 *Phys. Rev.* B **47** 7602
[5] Cardona M and Güntherodt G 1989 (ed) *Light Scattering in Solids V (Springer Topics in Applied Physics vol 66)* (Heidelberg: Springer)
[6] Cardona M 1990 *Superlatt. Microstruct.* **7** 183
[7] Klein M V 1986 *IEEE J. Quantum Electron.* **22** 1760
[8] Pinczuk A and Burstein E 1983 *Light Scattering in Solids I (Springer Topics in Applied Physics vol 8)* ed M Cardona (Heidelberg: Springer)
[9] Colvard C, Gant T A, Klein M V, Merlin R, Fisher R, Morkoc H and Gossard A G 1985 *Phys. Rev.* B **31** 2080
[10] Cros A, Cantarero A, Trallero-Giner C and Cardona M 1992 *Phys. Rev.* B **46** 12 627
[11] Shield A J, Trallero-Giner C, Cardona M, Grahn H T, Ploog K, Hoisler J A, Tenne D A, Moshegor N T and Toropov A 1992 *Phys. Rev.* B **46** 6990
[12] Sood A K, Menéndez J, Cardona M and Ploog K 1985 *Phys. Rev. Lett.* **54** 2111
[13] Bergues J M, Riera R, Comas F and Trallero-Giner C 1995 *J. Phys.: Condens. Matter* **7** 7273
[14] Bergues J M, Betancourt-Riera R, Marin J M and Riera R 1996 *Phys. Low-Dimens. Struct.* **7+8** 81
[15] Cardona M and Güntherodt G 1982 (ed) *Light Scattering in Solids II (Springer Topics in Applied Physics vol 50)* (Berlin: Springer)
[16] Bechstedt F, Enderlein R and Peuker K 1975 *Phys. Status Solidi* b **68** 43
[17] Comas F, Trallero-Giner C, Lang I G and Pavlov S T 1985 *Fiz. Tverd. Tela* B **27** 57 (Engl. Transl. 1985 *Sov. Phys.–Solid State* **27** 32)
[18] Goltzev A V, Lang I G and Pavlov S T 1979 *Phys. Status Solidi* b **94** 37
[19] Wallis R F and Mills D L 1970 *Phys. Rev.* B **2** 3312
[20] Riera R, Comas F, Trallero-Giner C and Pavlov S T 1988 *Phys. Status Solidi* b **148** 533
[21] Chamberlain P M, Trallero-Giner C and Cardona M 1995 *Phys. Rev.* B **51** 1680
[22] Sercel P C and Vahala K J 1990 *Phys. Rev.* B **42** 3690
[23] Fomin V M, Gladilin V N, Devreese J T, Pokatilov E P, Balaban S N and Klimin S N 1998 *Phys. Rev.* B **57** 2415
[24] Fomin V M, Pokatilov E P, Devreese J T, Klimin S N, Gladilin V N and Balaban S N 1998 *Solid-State Electron.* **42** 1309
[25] Comas F, Trallero-Giner C and Pérez-Alvarez R 1986 *J. Phys. C: Solid State Phys.* **19** 6479
[26] Comas F, Pérez-Alvarez R, Trallero-Giner C and Cardona M 1994 *Superlatt. Microstruct.* **14** 95
[27] Pérez-Alvarez R, García Moliner F, Velasco V R and Trallero-Giner C 1993 *J. Phys. C: Solid State Phys.* **5** 5389
[28] Chamberlain M P, Cardona M and Ridley B K 1993 *Phys. Rev.* B **48** 14 356
[29] Trallero-Giner C, García Moliner F, Velasco V R and Cardona M 1992 *Phys. Rev.* B **45** 11 944
[30] Jusserand B and Cardona M 1989 *Light Scattering in Solids V (Springer Topics in Applied Physics vol 66)* ed M Cardona and G Güntherodt (Heidelberg: Springer) p 61